Mapping distal femur fracture displacement fields and fixation plate deflection with weightbearing computed tomography

Thorhauer ED[1,2], Lack WD[1,3], Vazquez E[4], Davis J[4], Nelson S[4], Grantham A[1], Telfer S[1,2,3], Ledoux WR[1,2,3]
[1]RR&D Center for Limb Loss and MoBility (CLiMB), VA Puget Sound, Seattle, WA, [2]Department of Mechanical Engineering, University of Washington, Seattle, WA. [3]Department of Orthopaedics and Sports Medicine, University of Washington, Seattle, WA, [4]School of Medicine, University of Washington, Seattle, WA,
Email of Presenting Author: ericthor@uw.edu

Disclosures: Thorhauer ED (N), Lack WD (N), Vazquez E (N), Davis J (N), Nelson S (N), Grantham A (N), Telfer S (N), Ledoux WR (N)

INTRODUCTION: Distal femur fractures are uncommon but difficult injuries (8.7 per 100,000 person-years) with high rates of healing problems: while nonunion for long bones is 5–10%, complications in the distal femur have been reported up to 32% [1,2]. Clinical experience and prior work suggest fracture repair is strongly governed by local fracture biomechanics [3], yet we still lack practical tools to quantify how interfragmentary motion evolves in vivo under load, or how that motion relates to implant behavior and long-term outcomes [4]. Using weightbearing computed tomography (WBCT), our group has developed methods to capture three-dimensional fracture kinematics and strain fields. In this study we map displacement patterns (normal and shear) of distal femur fractures and, for plated constructs, quantify fixation-plate deflection during graded axial loading. We compare patterns across fixation types and materials and test whether plate bending correlates with local fracture site motion, providing construct-level insight that could inform implant choice and progression of weightbearing instructions.

METHODS: Seven cadaveric femurs (4M/3F; 2R/5L; 83.4 ± 5.7 years; 19.6 ± 2.9 BMI) underwent a standardized 10-mm metaphyseal gap osteotomy and fixation with either a lateral locking plate (n=6) or a retrograde intramedullary nail (n=1). Four radiopaque markers were embedded in both the proximal and distal fragments. Each limb was scanned with WBCT under six axial loads from 0 to 222.5 N in 44.5-N increments. Subject-specific fragment models from WBCT were rigidly registered to each scan using the markers, yielding relative fragment motion. Surface-to-surface displacement fields (Figure 1) across the gap were computed and decomposed into normal (compression/distraction) and shear components. For plated constructs, the implant was segmented on each scan, a subject-specific anatomical frame was established to standardize measurements, and the lateral plate edge deflection profiled to derive bending metrics. Associations between frontal plane plate bending angle and fracture-site motion across loads were evaluated with scatter plots and linear mixed-effects models (random intercept for subject). Pearson's correlation coefficients were computed for strain vs plate bending data.

RESULTS: Five plated limbs and one nailed limb were analyzed. Across plates, fracture-site motion scaled with plate bending: both absolute normal compression and absolute shear increased monotonically with increasing deflection (Figure 2). A stronger relationship between strain and plate bending was observed for normal (r = 0.776) compared to shear (r = 0.529). Material/working-length effects were evident: the titanium plate despite the shortest (46-mm) bridge span showed a more compliant response compared to stainless steel plates with longer bridge spans. The titanium nail produced the lowest and most uniform normal and shear motions, consistent with a stiffer, centralized load path. Displacement maps at maximal load demonstrated greater medial compression with lateral shear, consistent with subtle rotation about the femoral long axis under axial loading (Figure 1).

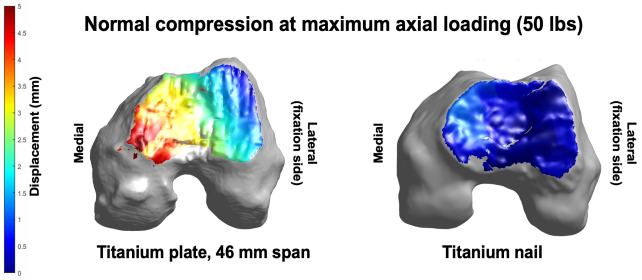

Figure 1: Example normal strain field: Ti plate (left) and Ti nail (right).

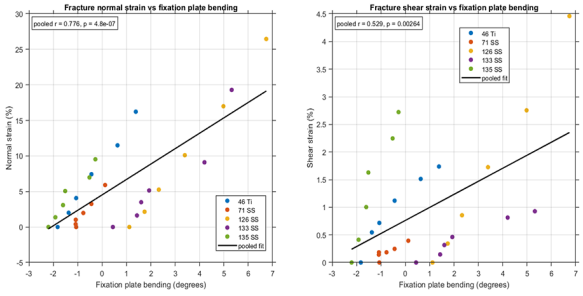

Figure 2: Fracture site strain vs plate deflection: normal (left) and shear (right). Fixation material and bridge span length (mm) are indicated in the legends.

DISCUSSION: WBCT-derived plate bending tracks with the magnitude of fracture-site motion. In lateral plates, bending increases both normal compression and shear at the fracture; the spatial pattern (medial compression with lateral shear) is consistent with a small rotation about the long axis of the femur. The titanium plate, despite being the shortest span, produced the largest motions, suggesting material compliance can outweigh working length (i.e., bridge span) in determining interfragmentary motion for lateral plates. By contrast, intramedullary nail fixation yielded lower, more uniform motions, aligning with its association with a more reliable and uniform fracture healing response.

Clinically, these mechanics align with the common observation of asymmetric callus under plates: higher medial compression is conducive to callus, whereas limited lateral compression and variable shear may suppress it. If borne out in larger samples, WBCT-based plate-bending measurements could provide a simple surrogate for in vivo interfragmentary motion, enabling operative decisions (material, bridge span, screw density) to be tuned toward healing-promoting biomechanical envelopes.

SIGNIFICANCE/CLINICAL RELEVANCE: WBCT enables non-invasive, standardized mapping of plate bending alongside interfragmentary compression and shear, directly quantifying the mechanical stimuli that contribute to fracture healing responses. By linking implant material/working length to fracture site motion, these metrics may guide construct selection, weightbearing progression, and early identification of subjects at risk for non-union.

REFERENCES: [1] Elsoe, R., et al., Int Orthop, 2018. 42(1): 191-6.; [2] Henderson, C.E., et al., J Orthop Trauma, 2011. 25 S1: S8-14.; [3] Kenwright, J. and A.E. Goodship, Clin Orthop Relat Res, 1989(241): 36-47.; [4] Inacio, J.V., et al., J Orthop Res, 2023. 41(5): 1049-59.

ACKNOWLEDGEMENTS: This work was funded by VA grants RX003608 and RX002970.